Recent Developments in Extracting the EOS from Observations

J. M. Lattimer

61st International Winter Meeting on Nuclear Physics
Bormio, Italy
27-29 January 2025

Acknowledgements

Funding Support:

DOE - Nuclear Physics

DOE - Toward Exascale Astrophysics of Mergers and Supernovae (TEAMS)

NASA - Neutron Star Interior Composition ExploreR (NICER)

NSF - Neutrinos, Nuclear Astrophysics and Symmetries (PFC - N3AS)

DOE - Nuclear Physics from Multi-Messenger Mergers (NP3M)

Recent Collaborators:

Boyang Sun (Stony Brook), Duncan Brown & Soumi De (Syracuse), Christian Drischler, Madappa Prakash & Tianqi Zhao (Ohio), Sophia Han (TDLI), Sanjay Reddy (INT), Achim Schwenk (Darmstadt), Andrew Steiner (Tennessee) & Ingo Tews (LANL)

Pulsar Timing for PSR J0737-3039

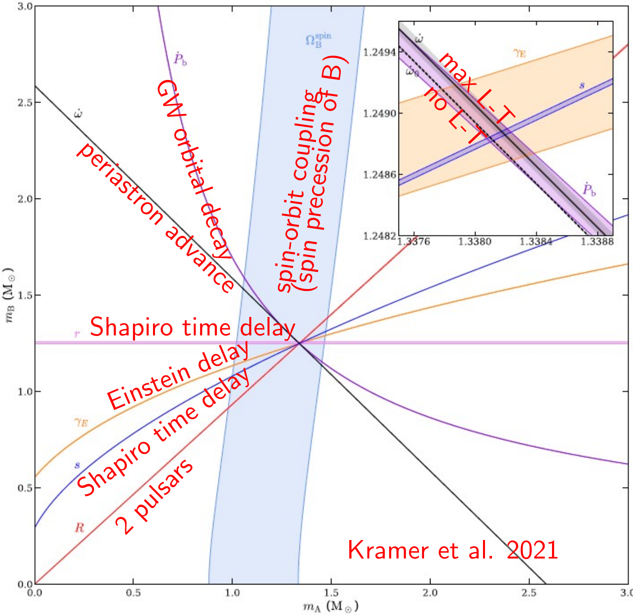

$m_A = 1.338185^{+12}_{-14}$ $M_\odot$
$m_B = 1.248868^{+13}_{-11}$ $M_\odot$

These are the most precisely known masses of any astronomical objects.

Masses of Pulsars in Binaries from Pulsar Timing

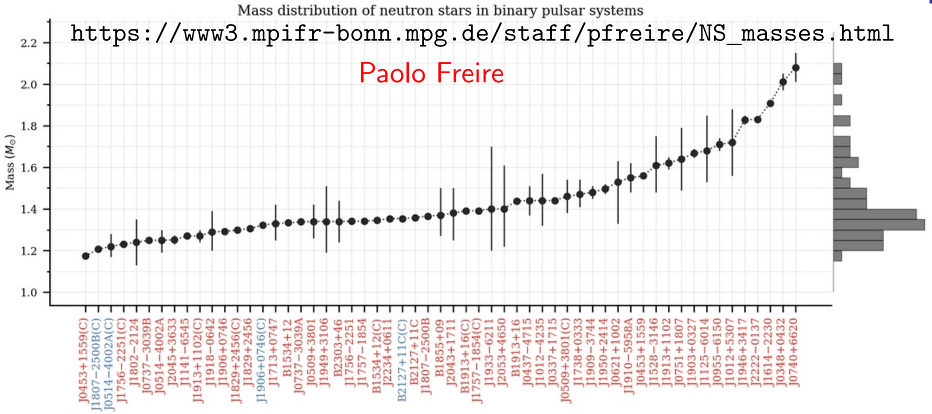

Largest: 2.08 ± 0.07 $M_\odot$
Smallest: 1.174 ± 0.004 $M_\odot$

Several other NS masses have been measured by other means, including some estimated to be more than $2M_\odot$ (e.g., black widow pulsars) and smaller than $1M_\odot$ (HESS J1731-347), but their mass uncertainties are generally large.

How Can a Neutron Star's Radius Be Measured?

- $\text{Flux} = \frac{\text{Luminosity}}{4\pi D^2} = \frac{4\pi R^2 \sigma_B T_s^4}{4\pi D^2} = \left(\frac{R}{D}\right)^2 \sigma_B T_s^4$
  X-ray observations of quiescent neutron stars in low-mass X-ray binaries measure the flux and surface temperature T_s. Distance D somewhat uncertain; GR effects introduce an M dependence.
- $F_{Edd} = \frac{GMc}{\kappa D^2}$ X-ray observations of bursting neutron stars in accreting systems measure the Eddington flux F_{Edd}. κ is the poorly-known opacity; GR effects introduce an R dependence.
- X-ray phase-resolved spectroscopy of millisecond pulsars with nonuniform surface emissions (hot spots). NICER: PSR J0030+0451, PSR J0437-4715 (closest and brightest millisecond pulsar) and PSR J0740+6620 (most massive pulsar).
- $R_{1.4} \simeq (11.5 \pm 0.3) \frac{\mathcal{M}}{M_\odot} \left(\frac{\tilde{\Lambda}}{800}\right)^{1/6} \text{km}, \quad \mathcal{M} = \frac{(M_A M_B)^{3/5}}{(M_A + M_B)^{1/5}}$
  GW observations of neutron star mergers measure the chirp mass $\mathcal{M}$ and binary tidal deformability $\tilde{\Lambda}$ (GW170817).
- $I_A \propto M_A R_A^2$ Radio observations of extremely relativistic binary pulsars measure masses M_A, M_B and moment of inertia I_A from spin-orbit coupling [PSR J0737-3039 ($P_b = 0.102$d), PSR J1757-1854 (0.164 d), PSR J1946+2052 (0.078 d)].

Neutron Star Interior Composition ExploreR (NICER)

Launched aboard a SpaceX Falcon 9 rocket on June 3, 2017.

It is installed aboard the International Space Station.

Dedicated to the study of neutron stars through soft X-ray timing.

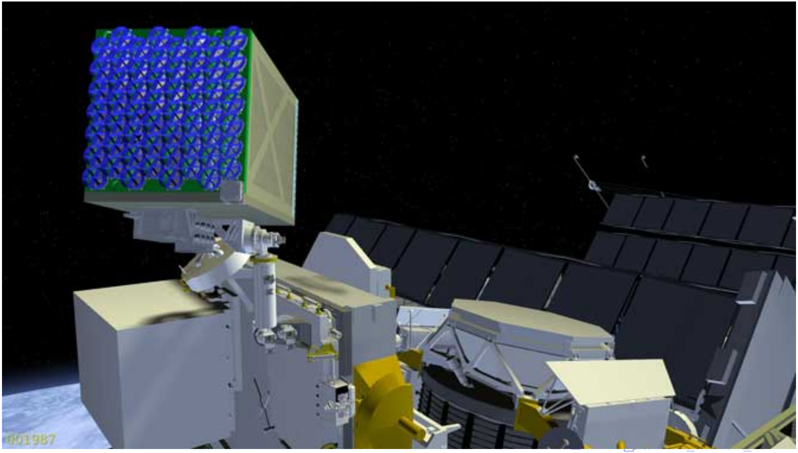

Science Measurements

NICER

Reveal stellar structure through lightcurve modeling, long-term timing, and pulsation searches

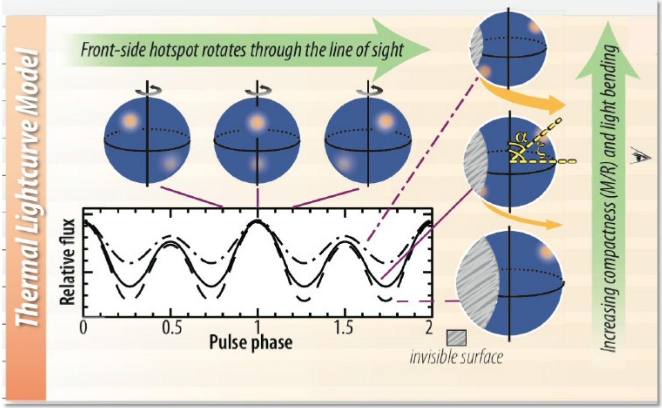

Lightcurve modeling constrains the compactness (*M/R*) and viewing geometry of a non-accreting millisecond pulsar through the depth of modulation and harmonic content of emission from rotating hot-spots, thanks to gravitational light-bending…

Science Measurements (cont.)

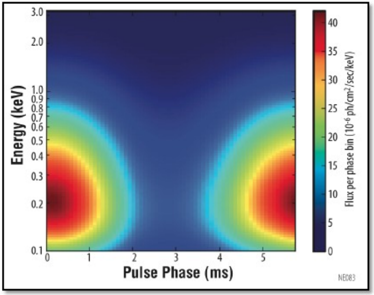

… while phase-resolved spectroscopy promises a direct constraint of radius *R*.

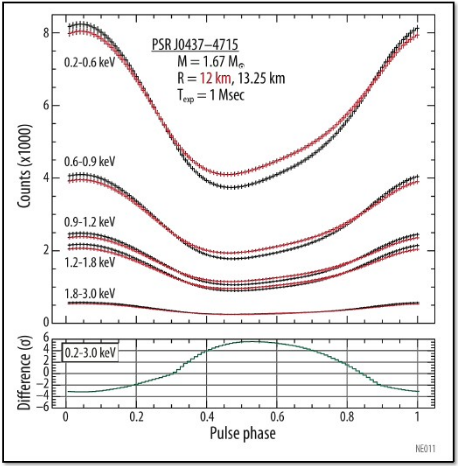

GW170817

- LVC detected a signal consistent with a BNS merger, followed 1.7 s later by a weak gamma-ray burst.
- $\sim$ 10100 orbits observed over 317 s.
- $\mathcal{M} = 1.186 \pm 0.001\ M_\odot$
- $M_{\rm T} = M_A + M_B \gtrsim 2^{6/5}\mathcal{M} = 2.725 M_\odot$
- $E_{\rm GW} > 0.025 M_\odot c^2$
- $D_L = 40^{+8}_{-14}$ Mpc
- $75 < \tilde\Lambda < 560$ (10.9 km$< \bar R <$13.3 km)
- $M_{\rm ejecta} \sim 0.06 \pm 0.02\ M_\odot$
- Blue ejecta: $\sim 0.01 M_\odot$
- Red ejecta: $\sim 0.05 M_\odot$
- Highly opaque ejecta implies substantial r-process production
- M_T+Ejecta+GRB: $M_{max} \lesssim 2.22 M_\odot$

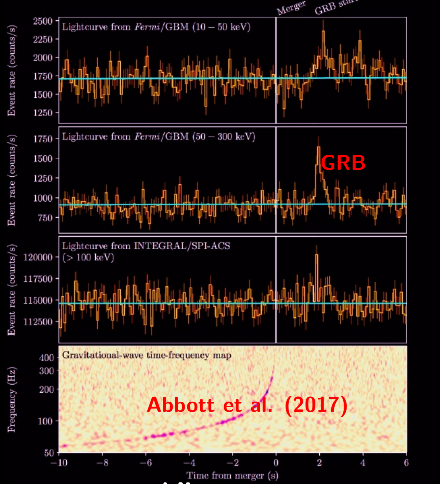

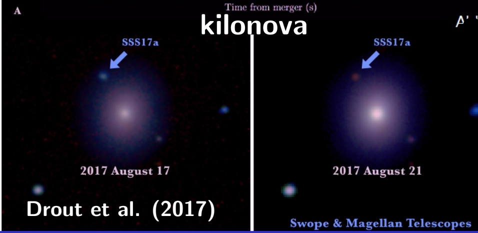

The Effect of Tides

Tides accelerate the inspiral and produce a gravitational wave phase shift compared to the case of two point masses.

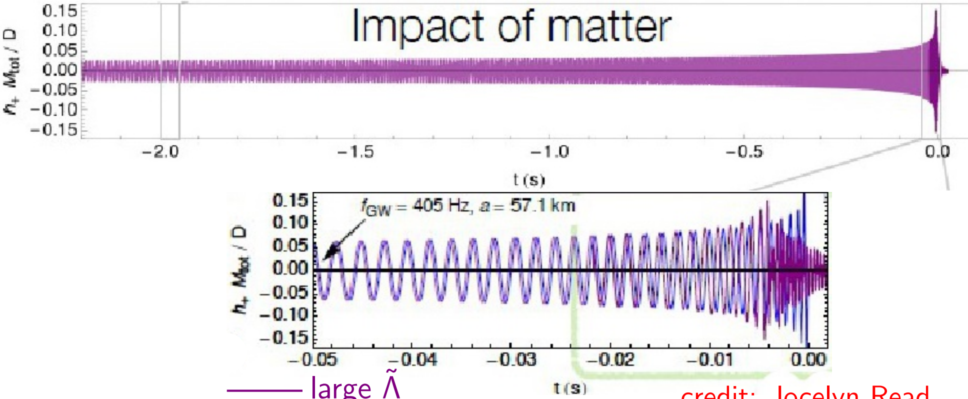

large $\tilde{\Lambda}$

small $\tilde{\Lambda}$

credit: Jocelyn Read

$$\delta\Phi_t = -\frac{117}{256}\frac{(1+q)^4}{q^2}\left(\frac{\pi f_{GW} G\mathcal{M}}{c^3}\right)^{5/3}\tilde{\Lambda} + \cdots .$$

Tidal Deformability

The tidal deformability λ is the ratio of the induced dipole moment Q_{ij} to the external tidal field E_{ij}, $Q_{ij} \equiv -\lambda E_{ij}$.

Use $\beta = GM/Rc^2$ and

$$\Lambda = \frac{\lambda c^{10}}{G^4 M^5} \equiv \frac{2}{3} k_2 \beta^{-5}.$$

$k_2 \propto 1/\beta$ is the dimensionless Love number, so $\Lambda \simeq a\beta^{-6}$. For $1 < M/M_\odot < 1.6$, $a = 0.0093 \pm 0.0007$.

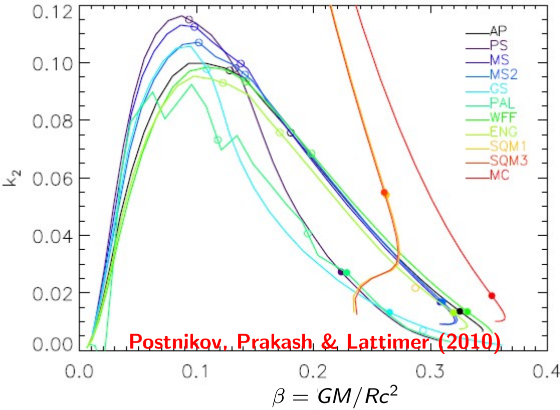

For a neutron star binary, the mass-weighted $\tilde{\Lambda}$ is the relevant observable:

$$\tilde{\Lambda} = \frac{16}{13} \frac{(1+12q)\Lambda_1 + (12+q)q^4\Lambda_2}{(1+q)^5}, \qquad q = M_2/M_1 \leq 1$$

Binary Deformability and the Radius

$$\tilde{\Lambda}=\frac{16}{13}\frac{(1+12q)\Lambda_1+q^4(12+q)\Lambda_2}{(1+q)^5}\simeq\frac{16a}{13}\left(\frac{R_{1.4}c^2}{G\mathcal{M}}\right)^6\frac{q^{8/5}(12-11q+12q^2)}{(1+q)^{26/5}}.$$

This is very insensitive to q for $q>0.5$, so

$$\tilde{\Lambda}\simeq a'\left(\frac{R_{1.4}c}{G\mathcal{M}}\right)^6.$$

For $\mathcal{M}=(1.2\pm0.2)\ M_\odot$, $a'=0.0035\pm0.0006$,

$$R_{1.4}=(11.5\pm0.3)\frac{\mathcal{M}}{M_\odot}\left(\frac{\tilde{\Lambda}}{800}\right)^{1/6}\mathrm{km}.$$

For GW170817, $\mathcal{M}=1.186M_\odot$, $a'=0.00375\pm0.00025$,

$$R_{1.4}=(13.4\pm0.1)\left(\frac{\tilde{\Lambda}}{800}\right)^{1/6}\mathrm{km}.$$

Moment of Inertia

- Spin-orbit coupling is of same magnitude as post-post-Newtonian effects (Barker & O'Connell 1975, Damour & Schaeffer 1988).
- Precession alters orbital inclination angle (observable if system is face-on) and periastron advance (observable if system is edge-on).
- More EOS sensitive than R: $I \propto MR^2$.
- Detection requires system to be extremely relativistic.
- Double pulsar PSR J0737-3037 ($P_b = 0.102$ d) is an edge-on candidate; $M_A = 1.338185 \pm 0.000004 M_\odot$.
- More relativistic systems have been found: PSR J1757-1854 ($M_A = 1.3412 \pm 0.0004 M_\odot$, $P_b = 0.164$ d) and J1946+2052 ($M_A < 1.31 M_\odot$, $P_b = 0.078$ d).
- Accurate (10%) I measurements expected by 2030 for both PSR J0737-3037 and J1757-1854.

Recent Moment of Inertia Measurement

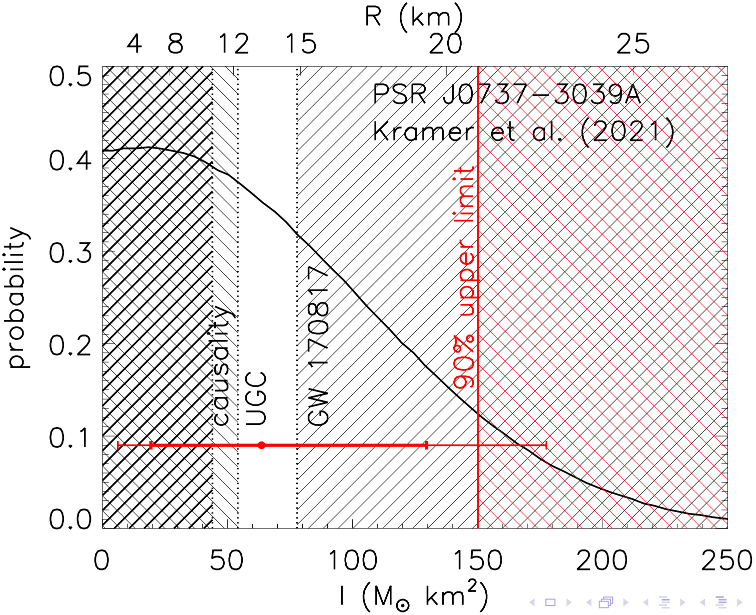

Constraints from Gamma-Ray Bursts

Quasi-periodic oscillations (QPOs) observed in short gamma-ray bursts (GRBs) are consistent with radial and quadrupolar vibrations of hypermassive neutron stars formed in the aftermath of neutron star mergers (**see Monday's talk by Cecilia Chirenti**).

Modeling indicates that quasi-universal relations connect the QPO frequencies with the chirp mass $\mathcal{M}$ and the binary tidal deformability $\tilde{\Lambda}$ for the merger. For the GRB 910711 (931101B), Guedes et al. (2025) infer $\mathcal{M} = 1.12^{+0.07}_{-0.05} M_\odot$ ($1.16^{+0.07}_{-0.07} M_\odot$) and $\tilde{\Lambda} = 683^{+188}_{-120}$ (528^{+137}_{-86}).

Assuming the progenitor systems were essentially identical and had mass ratios $q \simeq 1$, as is approximately the case for GW170817 and all observed galactic binary neutron stars, each progenitor star has

$$M = 2^{1/5}\mathcal{M} = 1.31 \pm 0.06 M_\odot, \quad \Lambda = \tilde{\Lambda} = 582 \pm 91.$$

Zhao & Lattimer (2018) found the semi-universal relation, valid for $1.2 \leq M/M_\odot \leq 1.6$:

$$\Lambda \simeq (0.0093 \pm 0.0007) \left(\frac{Rc^2}{GM}\right)^6,$$

yielding $R = 12.10 \pm 0.99$ km.

Summary of Astrophysical Observations

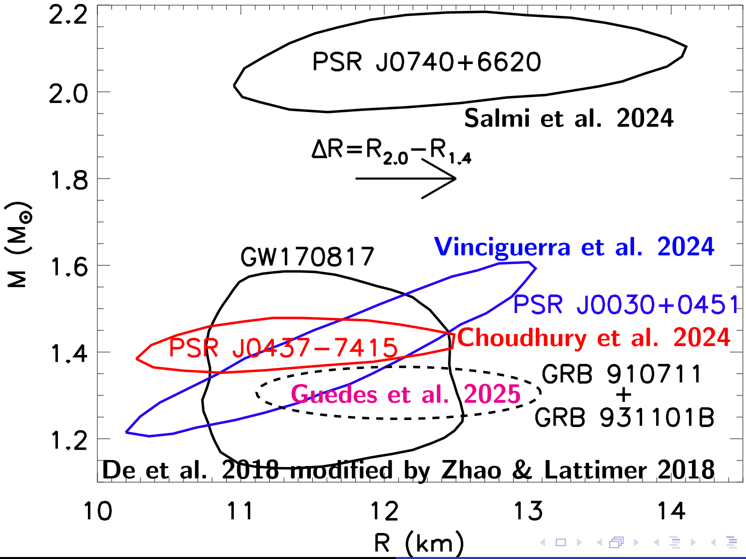

Nuclear Symmetry Energy and Pressure

The symmetry energy is the difference between the energies of pure neutron matter ($x = 0$) and symmetric ($x = 1/2$) nuclear matter:

$$S(n) = E(n, x = 0) - E(n, x = 1/2).$$

The quadratic term in an expansion of neutron excess $1 - 2x$ dominates:

$E(n, x) = E(n, 1/2) + (1-2x)^2 S_2(n) + \cdots$

Expanding S_2 about saturation n_s:

$$S_2(n) = \mathbf{J} + \frac{\mathbf{L}}{3}\frac{n - n_s}{n_s} + \ldots$$

$$\mathbf{J} \simeq 31 \text{ MeV}, \quad \mathbf{L} \simeq 50 \text{ MeV}$$

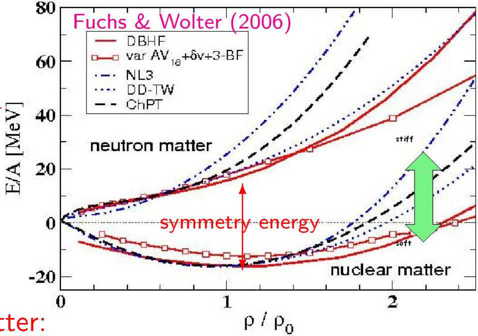

Extrapolated to pure neutron matter:

$$E_N = E(n_s, 0) \approx J + E(n_s, 1/2) \equiv J - B, \qquad P_N = P(n_s, 0) = L n_s/3$$

Neutron star matter (beta equilibrium) is nearly neutron matter:

$$\frac{\partial(E + E_e)}{\partial x} = 0, \quad P_{NSM}(n_s) \simeq \frac{L n_s}{3}\left[1 - \left(\frac{4J}{\hbar c}\right)^3 \frac{4 - 3J/L}{3\pi^2 n_s}\right]$$

Why is the Symmetry Energy Important?

The equation of state in a neutron star depends strongly on the density dependance of the symmetry energy ($u = n_B/n_s$):

$$P_{NSM}(u) \simeq n_s u^2 \left[\frac{L}{3} + \frac{K_N}{9}(u-1) + \frac{Q_N}{54}(u-1)^2 + \cdots\right].$$

A strong correlation exists between radii and P_{NSM} near n_s: $R_{1.4} \sim P_{NSM}(n_B)^{1/4}$.

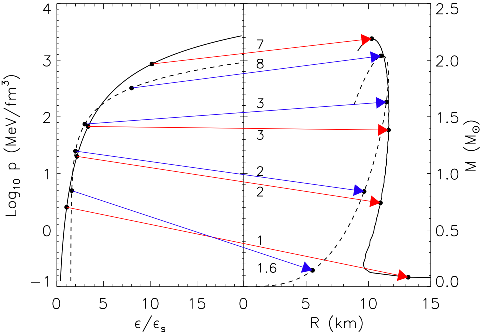

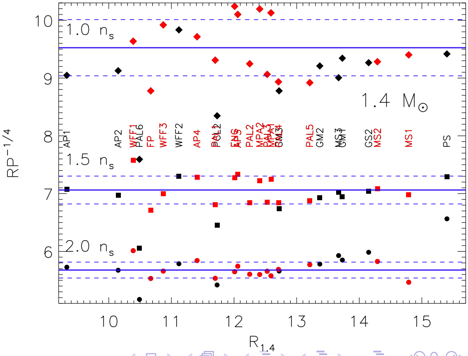

N3LO Chiral EFT Expansions

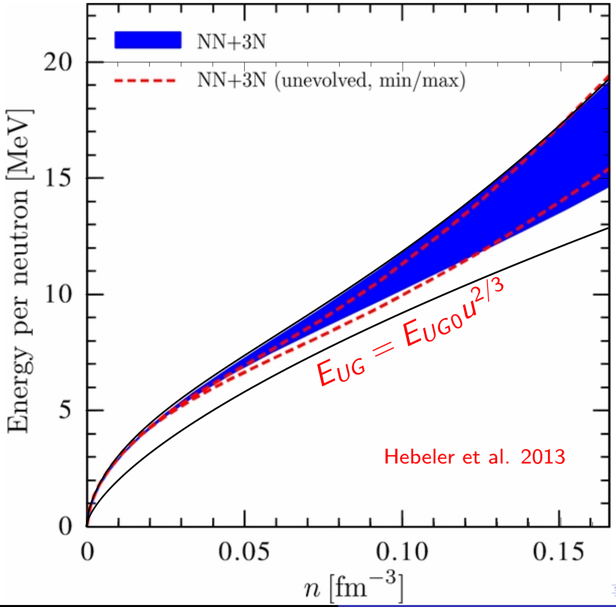

Bound From The Unitary Gas Conjecture

The Conjecture (UGC):
Neutron matter energy always larger than unitary gas energy.
$E_{UG} = \xi_0(3/5)E_F$, or

$$E_{UG} \simeq 12.6 \left(\frac{n}{n_s}\right)^{2/3} \mathrm{MeV}.$$

The unitary gas consists of fermions interacting via a pairwise short-range s-wave interaction with infinite scattering length and zero range. Cold atom experiments show a universal behavior with the Bertsch parameter $\xi_0 \simeq 0.37$.

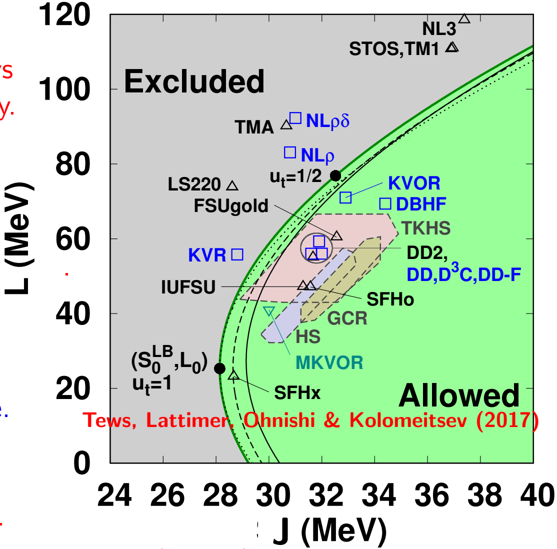

For $n \geq n_s$, one also observes $P_N > P_{UG}$ (UGPC).
$J \geq 28.6$ MeV; $L \geq 25.3$ MeV; $P_N(n_s) \geq 1.35$ MeV fm^{-3}; $R_{1.4} \geq 9.7$ km

What About An Upper Bound to E_{PNM}?

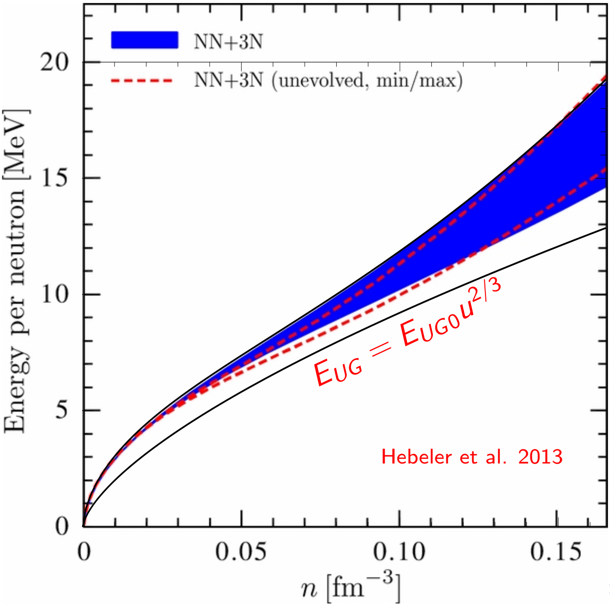

Imposing An Upper Neutron-Matter Energy Bound

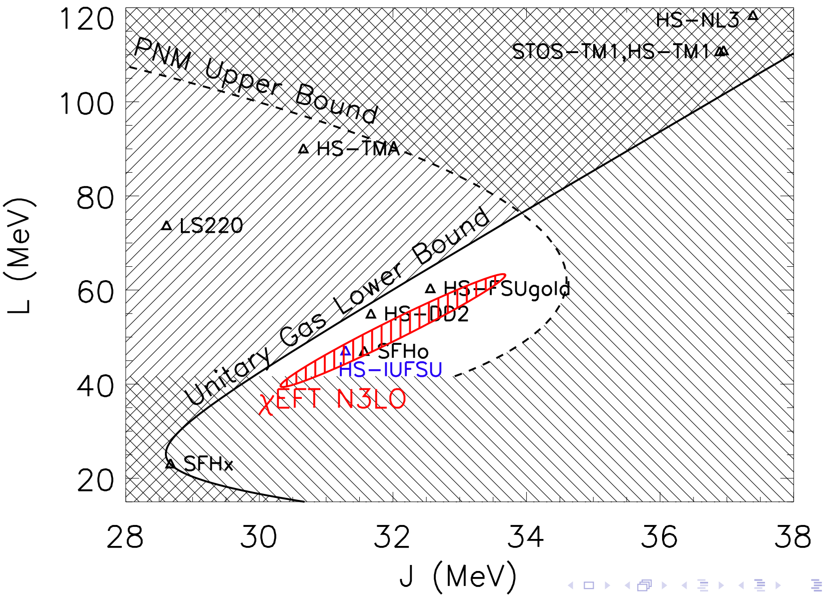

Unitary Gas Constraint Implications

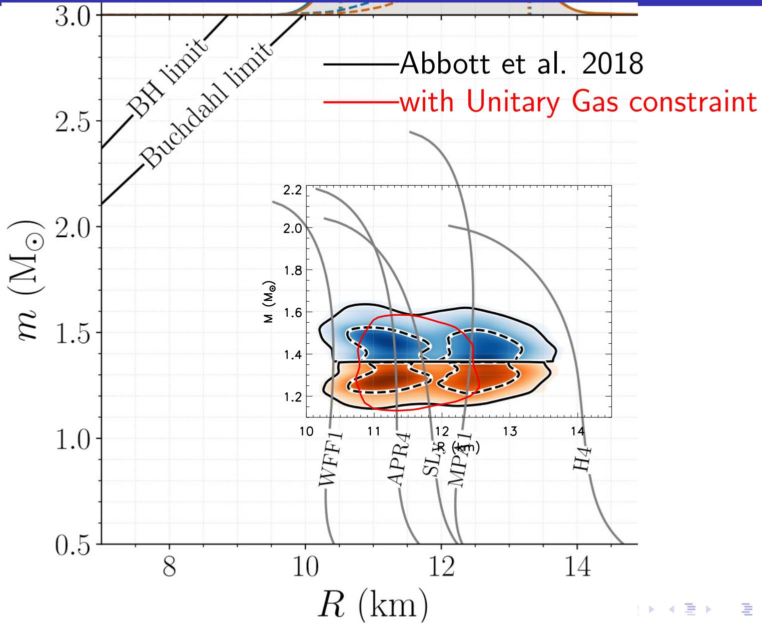

Importance of $\Delta R = R_{2.0} - R_{1.4}$

- J0437-4715: $R = 11.36^{+0.95}_{-0.63}$ km
- J0740+6620: $R = 12.49^{+1.28}_{-0.88}$ km

$\Delta R = +1.13^{+1.59}_{-1.08}$ km

313 Skyrme + RMF forces with $M_{max} \geq 2.0 M_\odot$

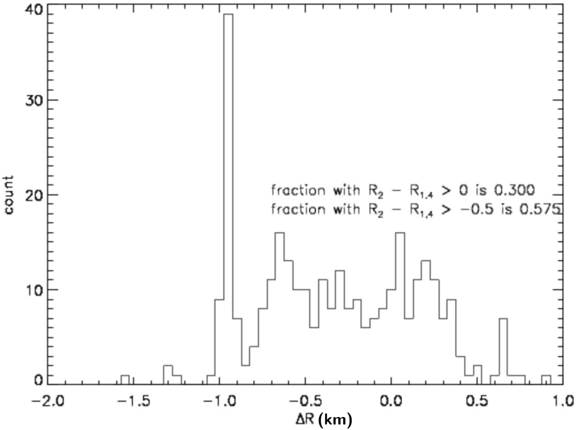

Neutron Star Structure

Tolman-Oppenheimer-Volkov equations

$$\frac{dp}{dr} = -\frac{G}{c^4}\frac{(mc^2+4\pi pr^3)(\varepsilon+p)}{r(r-2Gm/c^2)}$$
$$\frac{dm}{dr} = 4\pi\frac{\varepsilon}{c^2}r^2$$

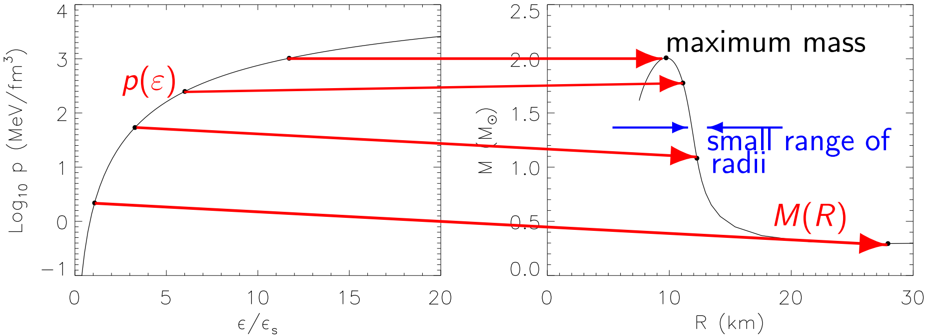

Equation of State ⟵ Observations

Maximum Mass As a Unique Scaling Point

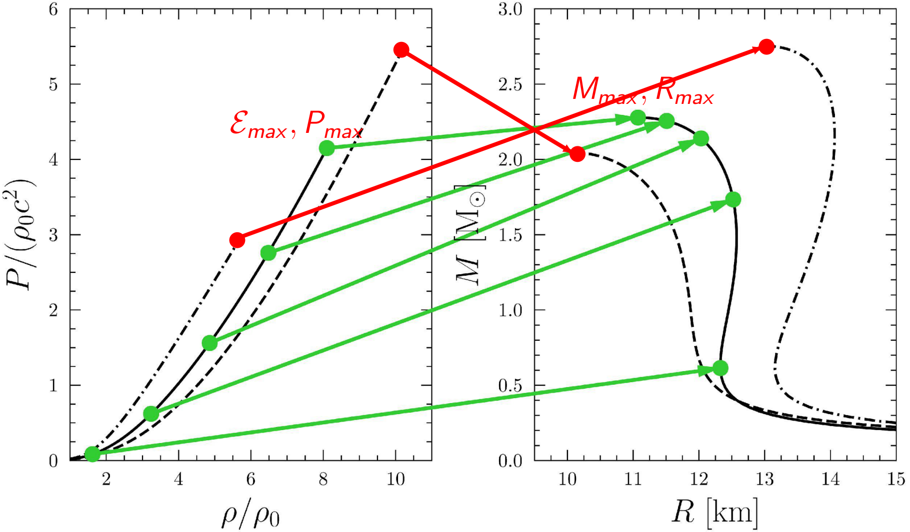

$M_{\max}$, $R_{\max}$, $\mathcal{E}_{\max}$, $P_{\max}$ Correlation

Ofengeim et al (2023) suggest power-law correlations

$$\mathcal{E}_{\mathrm{c,max}} = (1.809 \pm 0.36) \left(\frac{R_{\max}}{10\mathrm{km}}\right)^{-1.98} \left(\frac{M_{\max}}{M_\odot}\right)^{-0.171} \mathrm{GeV\ fm}^{-3},$$

$$P_{\mathrm{c,max}} = (118.5 \pm 6.2) \left(\frac{R_{\max}}{10\mathrm{km}}\right)^{-5.24} \left(\frac{M_{\max}}{M_\odot}\right)^{2.73} \mathrm{MeV\ fm}^{-3},$$

which are accurate to about 5% in fitting $\mathcal{E}_{c,max}$ and $P_{c,max}$.

Points along $M-R$ curves, at $M = fM_{\max}$, have similarly accurate correlations:

$$\mathcal{E}_{c,f} = a_{\mathcal{E},f} R_{fM_{max}}^{b_{\mathcal{E},f}} M_{max}^{c_{\mathcal{E},f}}$$

$$P_{c,f} = a_{P,f} R_{fM_{max}}^{b_{P,f}} M_{max}^{c_{P,f}}$$

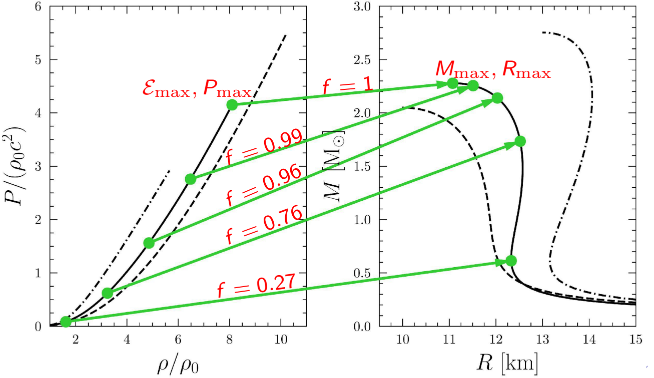

But (M, R) Is Not Equivalent To $(\mathcal{E}_c, P_c)$

While the maximum mass point (M_{max}, R_{max}) predicts $(\mathcal{E}_{c,max}, P_{c,max})$ to about 5%, and similarly for a given fractional maximum mass fM_{max}, the inversion is not unique. Two different equations of state predicting the same (M, R) (numbers in figure) arrive at those values from integration via different paths in $(\mathcal{E}, P)$ space. Similarly, two equations of state with identical values of $(\mathcal{E}_c, P_c)$ (letters) do not have the same (M, R) values.

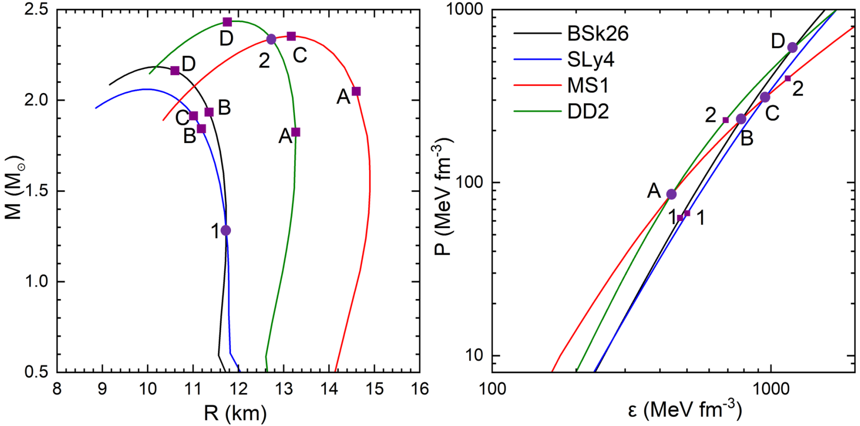

Correlations at $M = fM_{\rm max}$

Thus, more information than (M, R) needed. We find precision is greatly improved using a 2nd radius from a grid of fractional M_{max} points, *e.g.*, $f \in [1, 0.95, 0.9, 0.85, 4/5, 3/4, 2/3, 0.6, 0.5, 0.4, 1/3]$.

$$\mathcal{E}_f = a_{\mathcal{E},f}\left(\frac{R_{f_1}}{10\rm km}\right)^{b_{\mathcal{E},f_1}}\left(\frac{R_{f_2}}{10\rm km}\right)^{c_{\mathcal{E},f_2}}\left(\frac{M_{max}}{M_\odot}\right)^{d_{\mathcal{E},f}},$$

$$P_f = a_{P,f}\left(\frac{R_{f_1}}{10\rm km}\right)^{b_{P,f_1}}\left(\frac{R_{f_2}}{10\rm km}\right)^{c_{P,f_2}}\left(\frac{M_{max}}{M_\odot}\right)^{d_{P,f}},$$

$f = M/M_{\rm max}$	f_1	f_2	$\Delta(\ln \mathcal{E}_f)$	f_1	f_2	$\Delta(\ln P_f)$	$\Delta(\ln \mu_f)$	$\Delta(\ln n_f)$
1	0.95	3/5	0.00289	1	3/5	0.0117	0.00893	0.00401
0.95	0.95	3/4	0.00272	0.95	3/5	0.00701	0.00399	0.00289
0.90	0.95	2/3	0.00226	0.95	2/5	0.00518	0.00299	0.00239
0.85	0.95	1/2	0.00234	0.9	2/5	0.00489	0.00250	0.00234
4/5	0.9	1/2	0.00230	0.85	2/5	0.00462	0.00224	0.00230
3/4	0.85	1/2	0.00239	4/5	2/5	0.00539	0.00206	0.00243
2/3	3/4	1/2	0.00277	2/3	2/5	0.00511	0.00188	0.00257
3/5	3/4	2/5	0.00340	2/3	1/3	0.0172	0.00181	0.00315
1/2	2/3	1/3	0.00477	1/2	2/5	0.00998	0.00175	0.00457
2/5	1/2	1/3	0.00708	1/2	1/3	0.0188	0.00183	0.00672
1/3	1/2	1/3	0.0122	2/5	1/3	0.0259	0.00190	0.0119

greatly reduced uncertaintites!

Testing the Inversion

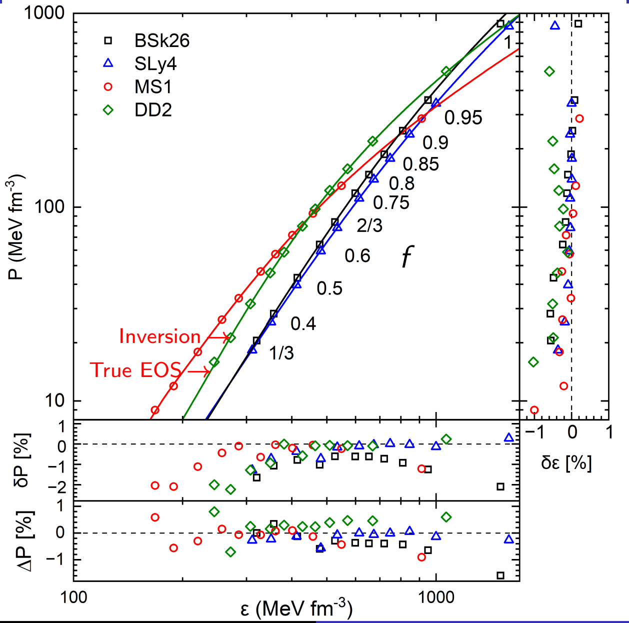

Testing the Inversion for $c_s^2 - P/\mathcal{E}$

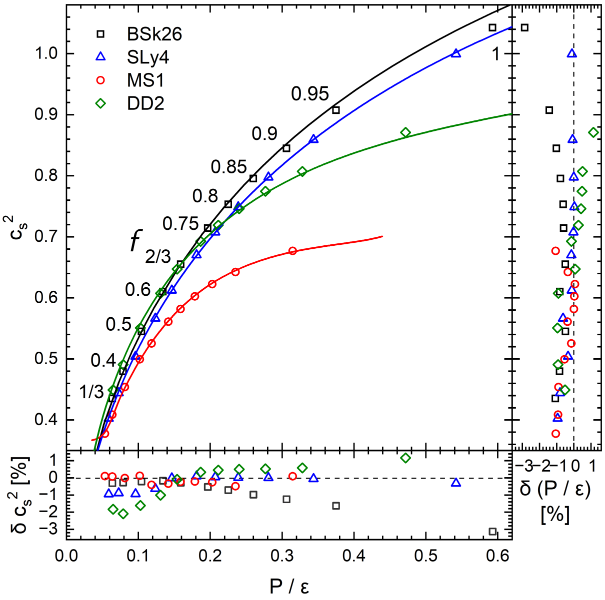

Inversions for μ and n

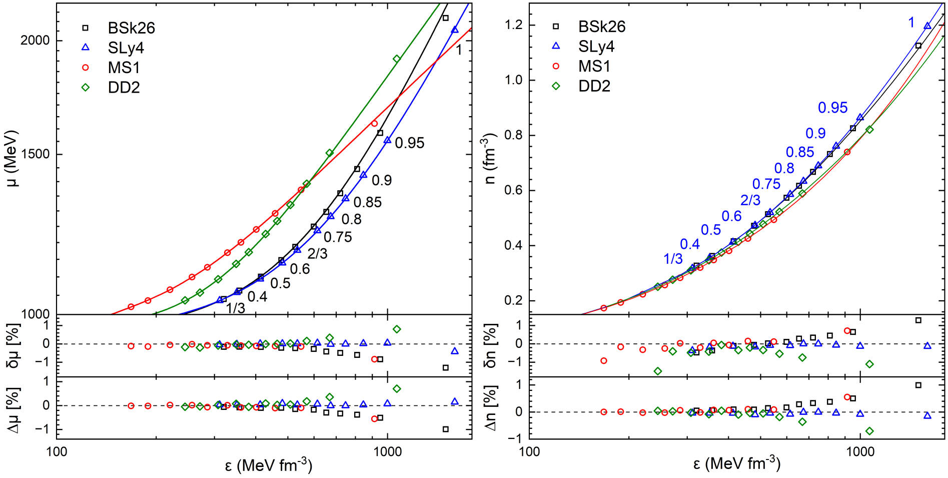

Inversions in Case of First-Order Transitions

Although fitting formulae were established using hadronic EOSs, they also work well in the case a first-order phase transition occurs. In this case, the reconstructed EOS smoothly bridges the phase transition.

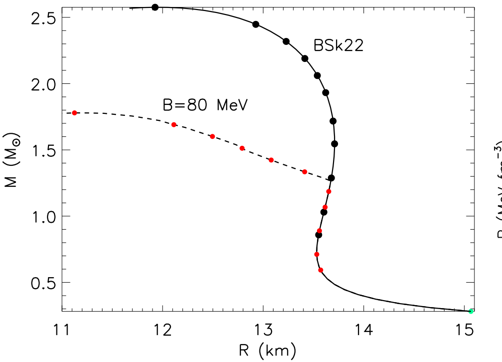

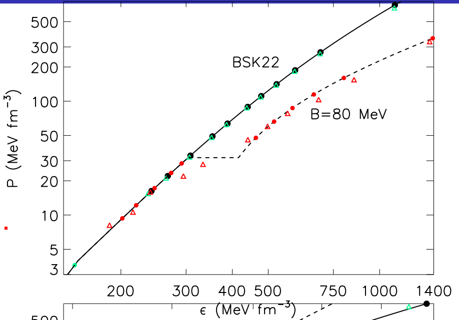

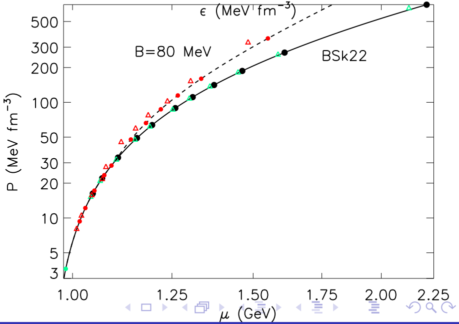

Inversion of $M - R$ Data

Instead of inverting an $M - R$ curve one may wish to infer the EOS from $M - R$ data. Traditional Bayesian inversions begin with $M - R$ priors generated by sampling millions of trials using a specific EOS parameterization with uniform distributions of parameters within selected ranges.

One problem with our approach is that M_{max} and R_{max} are not known. One can form analytical correlations between (M, R) and $(\mathcal{E}_c, P_c)$, but these have only moderate accuracy since this inversion is not unique. More information than the $M - R$ point itself is necessary to improve the inversion.

One possibility is to include the inverse slope dR/dM at the (M, R) point. Generally, one can determine a correlation between a quantity $G \in [\mathcal{E}_c, P_c, \mathrm{etc.}]$ and $(M, R, dR/dM)$ in the form

$$\ln G = \ln a_G + b_G \ln M + c_G \ln R + d_G(dR/dM).$$

Including dR/dM information improves correlations by factors of about 2. It is also found that inferred values of $\mathcal{E}_c$ and P_c are highly correlated; fits to $P_c/\mathcal{E}_c$ have much smaller uncertainty than fits to $\mathcal{E}_c$ or P_c.

Comparison to Traditional Bayesian Inference

From two $M - R$ regions obtained from observations select random pairs of points and determine dR/dM. Then, using the above correlation formulae, infer two $\mathcal{E}_c - P_c$ uncertainty regions (after rejecting pairs that violate the conditions $0 \leq dP_c/d\mathcal{E}_c \leq 1$ and $dP_c/dM > 0$).

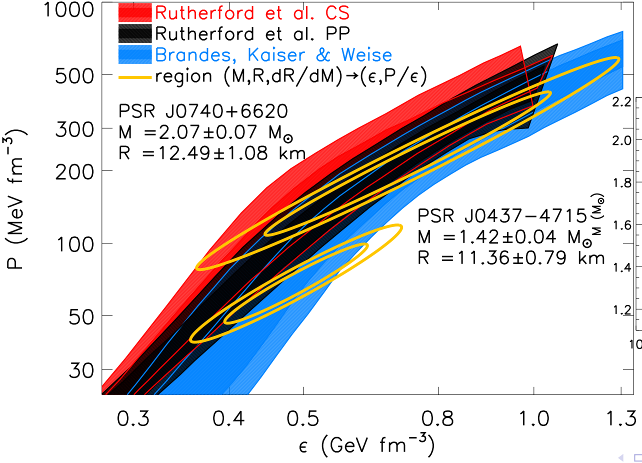

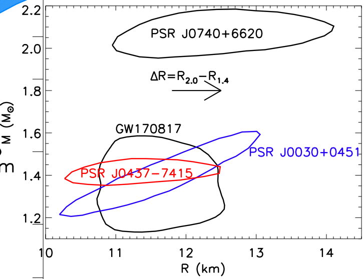

Applications

- Analytic inversion of TOV equations with arbitrarily high accuracies (depends on number of R_f values).
- Existing techniques use parameterized EOS models in probabilistic (Bayesian) approaches having unquantified systematic uncertainties stemming from the model and parameter choices (prior distributions).